Journal of Nuclear Materials 493 (2017) 322–329

Contents lists available at ScienceDirect

Journal of Nuclear Materials

journal homepage: www.elsevier.com/locate/jnucmat

Role of graphene layers on the radiation resistance of copper–graphene nanocomposite: Inhibiting the expansion of thermal spike

Hai Huang [a], Xiaobin Tang [a, b, *], Feida Chen [a], Jian Liu [a], Da Chen [a, b]

[a] Department of Nuclear Science & Engineering, Nanjing University of Aeronautics and Astronautics, Nanjing, 210016, China
[b] Jiangsu Key Laboratory of Nuclear Energy Equipment Materials Engineering, Nanjing, 210016, China

HIGHLIGHTS

- Metal–graphene nanocomposites are expected to have excellent radiation resistance.
- Graphene layers can greatly affect the performance of the composites.
- The effect reflected in reducing the scale of thermal spike induced by cascades.
- Three mechanisms (the intercept, recoil, and energy dissipation) can explain it.
- These mechanisms may provide a pathway to prevent material degradation.

GRAPHICAL ABSTRACT

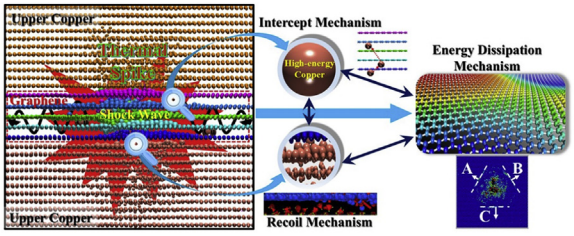

ARTICLE INFO

Article history:
Received 27 January 2017
Received in revised form
14 June 2017
Accepted 16 June 2017
Available online 21 June 2017

Keywords:
Copper–graphene nanocomposite
Graphene layers
Radiation resistance
Thermal spike
Molecular dynamics

ABSTRACT

Metal–graphene nanocomposites are expected to have excellent radiation resistance. The intrinsic role of the graphene layers (GrLs) in their performance has not been fully understood. Five copper–graphene nanocomposite (CGNC) systems were used to investigate the detailed mechanisms underpinning this behaviour by atomistic simulation. Results showed that GrLs can reduce the formation, growth, and intensity of the thermal spike of CGNC; this effect became more evident with the increasing number of layers of graphene. The role of the GrLs can be explained by three mechanisms: first, the ultra-strength C–C bonds of graphene hindered the penetration of high-energy atoms, second, the number of recoiled atoms decreased with the increasing number of layers of graphene, and third, the energy dissipation along the graphene planes also indirectly weakened the damage caused to the entire system. These mechanisms may provide a pathway to prevent material degradation in extreme radiation environments.

1. Introduction

In the next-generation of nuclear reactors, structural materials need to endure increased neutron doses for long periods of time without failure [1–3]. Moreover, long-term, or high dose-rate, radiation exposure is also a challenge to the survival of spacecraft [4]. Designing a material from the perspective of grain boundaries and

* Corresponding author. Department of Nuclear Science & Engineering, Nanjing University of Aeronautics and Astronautics, Nanjing, 210016, China.
E-mail address: tangxiaobin@nuaa.edu.cn (X. Tang).

http://dx.doi.org/10.1016/j.jnucmat.2017.06.023
0022-3115/

interfaces has gradually become a consensus among the scientific community with which it is hoped to improve the radiation tolerance of materials [5–11]. Graphene is characterised by a high Young's modulus (*c.* 1 TPa), high intrinsic strength (*c.* 130 GPa), and a low density [12]. The two-dimensional nanomaterial exhibits potential as a reinforcing component to be incorporated into metal matrices [12–14]. This disposition of the material can create a plentiful source of ultra-high strength metal–graphene interfaces and confer pure metals with novel functions [14–16]. Excellent radiation tolerance may be one of the most outstanding features of metal–graphene nanocomposites. Thus, metal–graphene nanocomposites are very promising structural materials for nuclear engineering applications.

Several irradiation experiments [17,18] and simulations [19,20] have been carried out to verify the performance of metal–graphene nanocomposites. Kim et al. [17] performed He^+ irradiation experiments on vanadium–graphene nanocomposite; the resulting composite exhibits higher radiation tolerance than its pure counterpart. Si et al. [18] found that a smaller-period-thickness tungsten–graphene nanocomposite exhibits high radiation tolerance in the reduction of He-bubble density. By *ab initio* calculations, Yang et al. [19] demonstrated that the interface in the copper–graphene nanocomposite (CGNC) provides a strong sink for trapping defects and gives rise to preferential sites for their recombination. In our previous work, a CGNC system under collision cascades was investigated by atomistic simulation [20]. The simulation results showed that the surviving defects in the bulk region of CGNC are always fewer in number than those in pure copper. These results highlight the radiation tolerance of metal–graphene nanocomposites; however, to our knowledge, many radiation effects of the materials described in the previous studies were simply attributed to the original design concept, *viz.*, the "self-healing" ability of irradiated defects being improved by the presence of interfaces [2,5–7,10,11]. As a result, the intrinsic role of the graphene layers (GrLs) in reducing the formation of radiation-induced crystalline defects is neglected.

In this work, a series of molecular dynamics (MD) simulations were performed to assess the effects of GrLs (including 1-, 2-, 3-, 5-, and 8-layer graphene) on the radiation resistance of CGNC under irradiation. The reason that copper was used as the matrix material has been given in our previous work [21]. This paper is organised as follows: the defect evolution and atom displacement in different CGNC systems were investigated, then the mechanisms through which the GrLs of CGNC affected the formation of radiation-induced defects were identified. Our results highlight the role of the GrLs in reducing the formation, growth, and intensity of displacement cascades of CGNC in the thermal spike phase.

2. Simulation methodology

Five CGNC structures (Fig. 1), which differed in the number of layers of graphene therein, *viz.*, 1-, 2-, 3-, 5-, and 8-layer graphene, were generated in this work (detailed configurations are provided in the Supplementary Material). Different names for these configurations are respectively defined as: Cu/Gr/Cu, Cu/2Gr/Cu, Cu/3Gr/Cu, Cu/5Gr/Cu, and Cu/8Gr/Cu. The interactions among carbon atoms (C–C) in the GrLs were described by the adaptive intermolecular reactive empirical bond order (AIREBO) potential [22], which is widely used in radiation damage studies of graphene [23–25]. The embedded atom method (EAM) potential, splined to the Ziegler–Biersack–Littmark (ZBL) repulsive potential, was used to describe the interactions between copper atoms (Cu–Cu) [26]. In describing the interactions between copper and carbon atoms (Cu–C), the 12–6 Lennard–Jones (LJ) type of van der Waals interactions was used. The LJ potential has been used to simulate

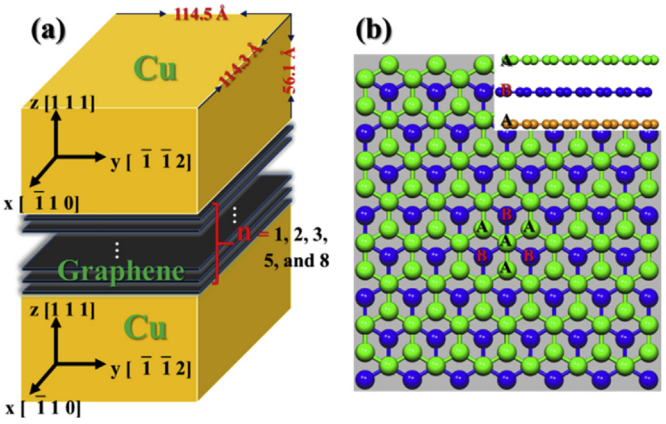

Fig. 1. (**a**) Conceptual schematic diagram representing the simulation cell of Cu/Gr/Cu, Cu/2Gr/Cu, Cu/3Gr/Cu, Cu/5Gr/Cu, or Cu/8Gr/Cu. (**b**) Top view of 3-layer graphene. The green and blue atoms represent the top and middle layers, respectively. The inset offers a lateral view, in which the yellow atoms represent the bottom layer. The stacking configuration of multi-layer graphene contained in the model shown in panel (a) is a Bernal AB-bilayer type, which has been explained in the Supplementary Material. (For interpretation of the references to colour in this figure legend, the reader is referred to the web version of this article.)

cascade collisions of vanadium–graphene nanocomposite by Kim et al. [17]. Their simulation results are consistent with experimental observations, confirming the feasibility of the potential in cascade simulations of metal–graphene nanocomposites. The parameters (the well depth $\sigma_{(Cu-C)}$ = 3.225 Å, equilibrium distance $\varepsilon_{(Cu-C)}$ = 0.019996 eV, and cut-off radius $r_c = 2.5\sigma_{(Cu-C)}$) used in this work were derived from density functional theory (DFT) calculations [27].

Initially, each model was relaxed at the NVT ensemble (constant number of atoms, volume, and temperature) for 10 ps until each system reached a stable state. The temperature was set to 300 K in this process. Subsequently, a primary knock-on atom (PKA) with 3.0 keV was introduced at a certain distance (d = 15.4 Å) from its nearest graphene plane and directed toward its copper–graphene (Cu–C_gr) interface (see Fig. S2). More simulation settings can been found in the Supplementary Material. The distance (d = 15.4 Å), incidence direction, and energy of PKA were adopted in each model to ensure that the centre of the displacement cascades in each model is as close to its GrLs as possible. This disposal approach makes it easy to distinguish the effects of the number of layers of graphene on the displacement cascades. In addition, 10 independent cascade simulations were performed in each model to reduce the statistical error in the result.

Before cascades, the interface (containing GrLs and two terminal copper planes near the GrLs) and bulk (containing all of copper atoms apart from those of interface) regions of CGNC were distinguished. The methods of definition of different regions have been depicted in the Supplementary Material. After cascades, the reference lattice site method at a cut-off distance of $0.3a_0$ (a_0 is the lattice constant of copper) was used to characterize the defects of bulk region in the five CGNC systems [5]. All simulations were performed with the MD code LAMMPS [28] and visualisations were rendered with OVITO [29].

3. Results

3.1. Evolution of point defects

Fig. 2 presents the typical time evolution of the number of point defects during displacement cascades. These profiles are consistent

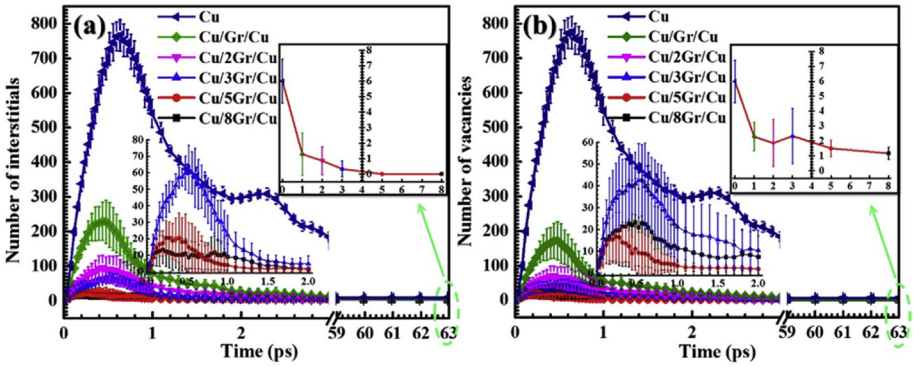

Fig. 2. Time evolution of the number of (**a**) interstitials and (**b**) vacancies produced in the bulk region of each CGNC, as well as pure copper during the displacement cascades. The number of final stable defects is shown in the inset. For the Cu/3Gr/Cu, Cu/5Gr/Cu, and Cu/8Gr/Cu, their time evolution of defects near the peak position is magnified.

with the behaviours observed in other materials [30,31]. For clarity, a mean of 10 runs of each CGNC system is plotted. The number of defects in the bulk region of each CGNC increased rapidly in the beginning and reached its maximum value thereafter. The time to peak defect count for each CGNC was in the range of 0.2–0.4 ps and was delayed with decreasing number of layers of graphene, which may attribute to the role of GrLs in reducing thermal spike relative to that of metals [32]. Eventually, most of defects in each CGNC recombined or were trapped by the Cu–C_gr interface [19]. Very few of them remained as stable defects in their bulk region at approximately 63 ps. A similar trend also appears in pure copper.

However, most clearly, a significant contrast between CGNC and pure copper occurs near the peak position. In addition, the peak defect count of pseudo bulk region of pure copper was also compared with that of corresponding bulk region of CGNC (depicted in Fig. S3). All of the peak values of defect counts in the five CGNCs were much less than that in pure copper. This result highlights the role of the GrLs in decreasing defects in the thermal spike phase. For example, the peak value of defect count in Cu/Gr/Cu relative to that of pure copper decreased to approximately 25%, and it decreased to approximately 12.5% for Cu/2Gr/Cu compared with pure copper. In addition, the peak position of pure copper at approximately 0.6 ps was delayed in contrast to those of the CGNCs. This result suggests the function of the GrLs lay in a weakening of the ballistic phase. The tendency that more layers of graphene exhibited lower defect count peak emerged in the five CGNCs analysed. This phenomenon implied a synergistic interaction between different graphene planes on decreasing defect count in the thermal spike phase. Moreover, the defect concentrations in the five CGNCs quickly tended towards stability and did so more rapidly than that of pure copper. The final stable defect productions also exhibited a similar tendency to that of the peak value of the defect counts in different models, implying a correspondence between the peak defect counts and the number of final surviving defects. This phenomenon can give us some quantitative indication of the differences arising from the use of different numbers of layers of graphene on the radiation resistance of CGNC.

3.2. Defect distribution and atom displacement at the thermal spike

The peak defect count in the lower or upper bulk region of each CGNC *versus* the number of layers of graphene is shown in Fig. 3 to reveal the source of the defect reduction in CGNC. Obviously, the increase in the number of layers of graphene will gradually decrease the number of defects in both the lower, and upper, bulk regions of CGNC. The decreased number of defects in the upper bulk region is reasonable as the number of layers of graphene

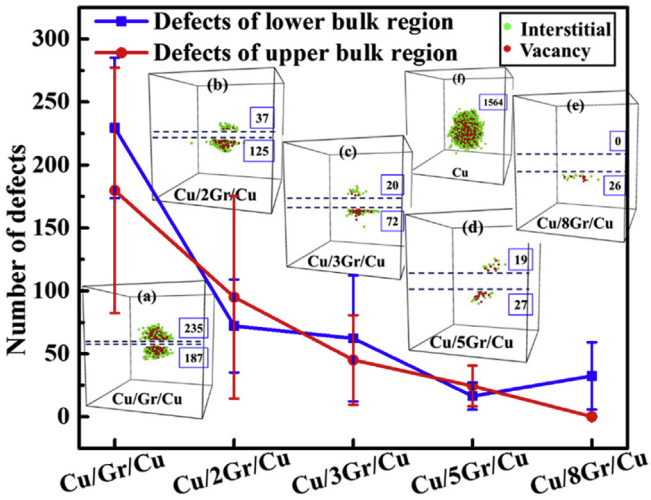

Fig. 3. The peak defect count (containing interstitials and vacancies) in the lower or upper bulk region of each CGNC, respectively. Snapshots of the defect distribution of the bulk region of CGNC at the moment are shown in the inset of panels ((a) Cu/Gr/Cu, (b) Cu/2Gr/Cu, (c) Cu/3Gr/Cu, (d) Cu/5Gr/Cu, or (e) Cu/8Gr/Cu). As a contrast, a snapshot of the defect distribution of pure copper at the moment is also shown in the inset of panel (f). The green and red spheres represent interstitials and vacancies in the cells, respectively. The interface region is marked by two dashed blue lines. Several Arabic numerals in the cells show the sum of interstitials and vacancies in the lower, or upper, bulk region of each CGNC. (For interpretation of the references to colour in this figure legend, the reader is referred to the web version of this article.)

increased because of the continuous reinforcement of the graphene interception effect; however, the obvious decrease in the number of defects in the lower bulk region is least likely to occur. The reason is that a PKA in each model was introduced at the same distance relative to its nearest graphene plane and should induce, by rights, approximately the same number of defects in the lower bulk region of each CGNC. The snapshot of the defect distribution of pure copper at the moment of peak defect count is shown in Fig. 3(f). The large number of defects in pure copper relative to that of CGNC highlights the significant role of the GrLs in inhibiting defect formation in the thermal spike region.

The image of atom displacement of each model near Cu–C_gr interface is shown in Fig. 4(a–e). Atom displacement in each image is visualised by showing the displacement vectors between atomic positions at 0 and 63 ps. These lattice points in Fig. 4 represent copper or carbon atoms. Each red line represents a displacement vector of an atom. The head of each line is an initial position of an atom, whereas the tail is the final position thereof. An atom that

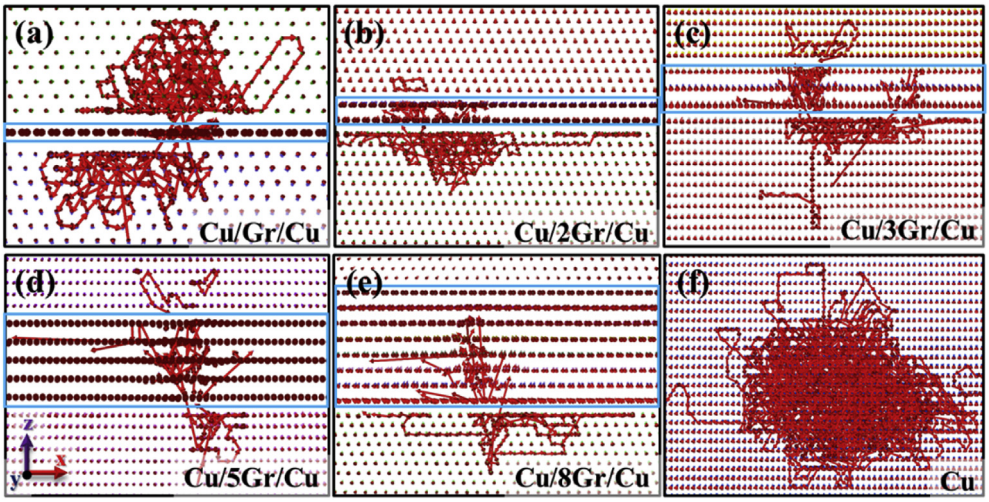

Fig. 4. Projection views of thermal spike region in (**a**) Cu/Gr/Cu, (**b**) Cu/2Gr/Cu, (**c**) Cu/3Gr/Cu, (**d**) Cu/5Gr/Cu, (**e**) Cu/8Gr/Cu, and (**f**) pure copper. Atom displacement in each image is visualised by showing the displacement vectors between atomic positions at 0 and 63 ps. The lattice points represent copper or carbon atoms. The red lines represent displacement vectors of the atoms. The region of GrLs is identified by a blue box. (For interpretation of the references to colour in this figure legend, the reader is referred to the web version of this article.)

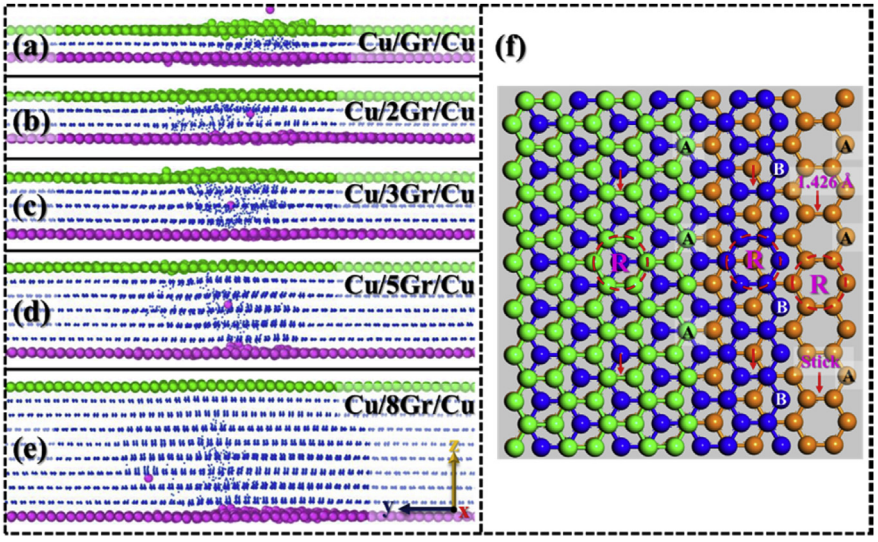

Fig. 5. Projection views of the interface regions of (**a**–**e**) five CGNCs in the thermal spike phase. The penetrable copper atoms from their lower bulk region are also shown. (**f**) The top view of 3-layer graphene with AB-bilayer stacking. In panels (a–e), the pink, green, and blue spheres represent copper and carbon atoms, respectively. In panel (f), different coloured spheres represent carbon atoms in different layers. These sticks represent hypothetical C–C bonds. The size of spheres is not fixed for ease of visualization. (For interpretation of the references to colour in this figure legend, the reader is referred to the web version of this article.)

almost overlaps with its displacement vector indicates a slight fluctuation of the atom around its lattice position. A long line represents a large atom displacement. The continuous lines made of series of displacement vectors show a replacement collision sequence (RCS). Eventually, the thermal spike region of each model is visualised by these disordered, or overlapping, lines. Two characteristics are the most distinct with the increasing number of layers of graphene in the thermal spike region of CGNC. On the one hand, the number of RCS gradually decreases and the number of individual long-range displacements increases. On the other hand, the extent of overlaps between different displacement vectors gradually decreases and each displacement vector becomes distinguishable. In addition, the tendency of the size of thermal spike region is consistent with that of the defect distribution in the lower, or upper, bulk region of CGNC. The image of atom displacement of pure copper is shown in Fig. 4(f). The significant amount of overlaps between displacement vectors, as well as the large displacement range in the thermal spike region of pure copper, implies that the GrLs exhibited the ability to prevent copper atoms of CGNC from deviating from their lattice points.

4. Discussion

The results shown in Figs. 2–4 indicate that the GrLs play an important role in weakening the formation, growth, and intensity of the thermal spike region of CGNC. Three different mechanisms corresponding to different regions are discussed in the following sub-sections, revealing the detailed role of the GrLs.

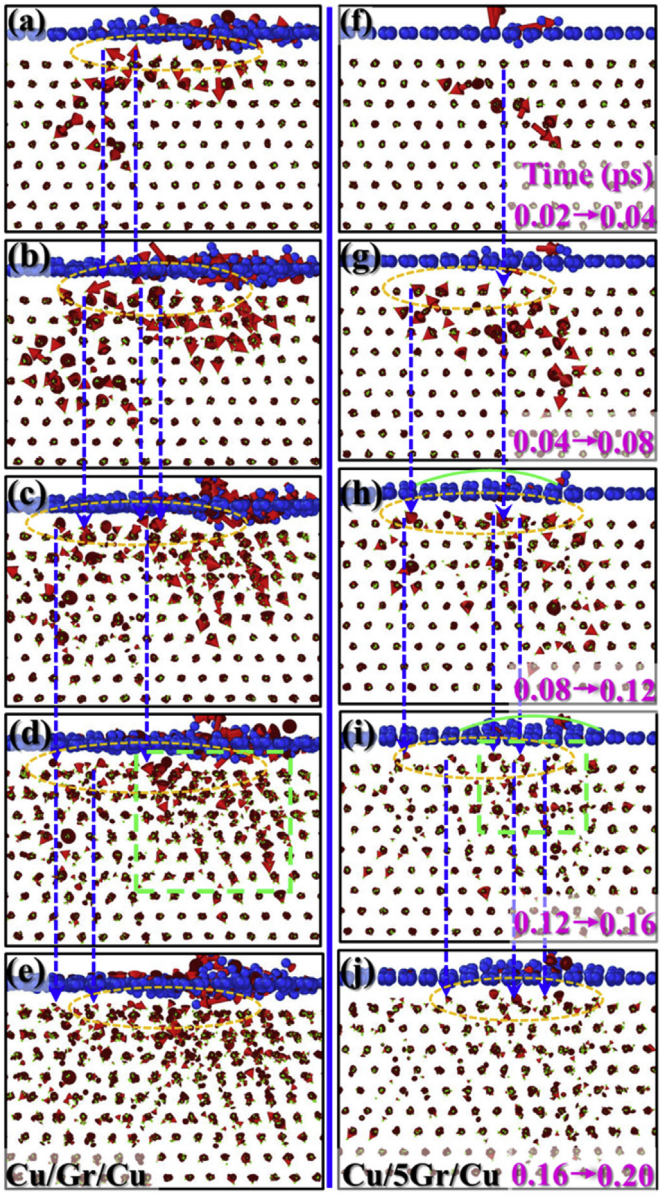

Fig. 6. Evolution of atom displacement in the lower bulk region and its nearest graphene plane in (**a**–**e**) Cu/Gr/Cu and (**f**–**j**) Cu/5Gr/Cu, respectively. Atom displacement in each image is visualised by showing the displacement vectors between atomic positions in various time intervals (0.02 or 0.04 ps). The descriptions of lattice points and red lines are similar to those in Fig. 4. Several of the same atoms in different images are connected with blue lines so as to observe the evolution of atomic positions. These recoiled atoms in the gap between graphene and copper are marked by a yellow oval. The bend in the graphene of Cu/5Gr/Cu is marked by a green curve. The size of the spheres is not fixed for ease of visualization. (For interpretation of the references to colour in this figure legend, the reader is referred to the web version of this article.)

4.1. Upper bulk region of CGNC

The high energy atoms including PKA and secondary knock-on atoms originating from the lower bulk region can break the siege of interface and induce damage in the upper bulk region. Fig. 5(a–e) show the Cu–C_gr interface region of each CGNC and the penetrable copper atoms from their lower bulk region in the thermal spike phase. These copper atoms are obviously intercepted by graphene, while the effect becomes weak in pure copper as shown in Fig. S4. This may be the difference of physical and

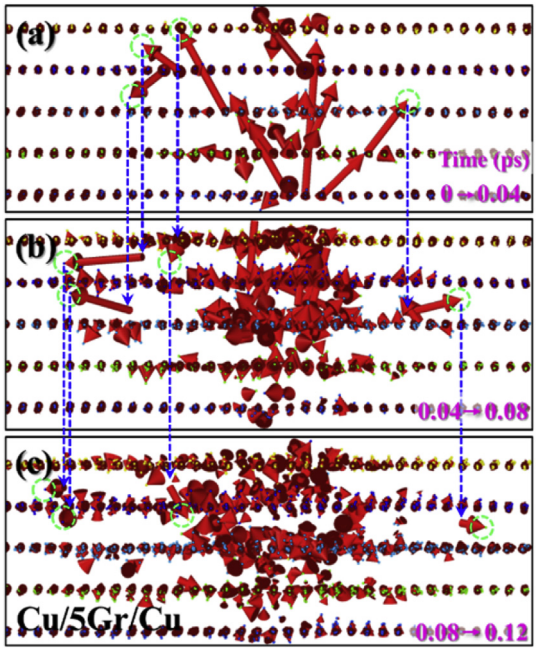

Fig. 7. Evolution of atom displacement in the GrLs of Cu/5Gr/Cu. Atom displacement in each image is visualised by showing the displacement vectors between atomic positions in a time interval of 0.04 ps. The descriptions of lattice points and red lines are similar to those in Fig. 4. Several of the same atoms in different images are connected by blue lines to allow clear observation of the evolution of the atomic positions. (For interpretation of the references to colour in this figure legend, the reader is referred to the web version of this article.)

chemical property between graphene and copper. The cohesive energy of graphene (−7.81eV/atom) is much greater than that of pure copper (−3.53 eV/atom) as shown in Fig. S1. The displacement energy (E_d, 25–28 eV [32,33]) and the enthalpy of atomization (EA, 717 kJ/mol [34])of graphene are also greater than those of pure copper (EA, 338 kJ/mol [34]; E_d, 18.3 eV [35]). These can generate ultra-strength C–C bonds for graphene, which allows these atoms to penetrate the graphene plane at the centre of each ring (R) easily but with more difficulty at other positions. This has been verified by the results arising from the irradiation of graphene with carbon ions [36]. As a result, damage was less in the upper bulk region of CGNC relative to that of pure copper.

Only one copper atom successfully entered its upper bulk, or interface, region in each CGNC in the thermal spike phase. The penetrable atom in the Cu/Gr/Cu continued causing damage to its upper bulk region. However, the penetrable atom in other CGNCs was retained in its GrLs. Moreover, the carbon atoms of top graphene plane were displaced to strike copper atoms above the GrLs because of the knock-on of the penetrable copper atom in each CGNC. Different levels of damage in the upper bulk regions, depending on the kinetic energy of these carbon atoms, occurred subsequently. None of the displaced carbon atoms in the GrLs of each CGNC escaped from their GrLs: this phenomenon highlighted the role of the C–C bonds of graphene in inhibiting the damage to the upper bulk region. With an increasing number of layers of graphene, penetrable copper atoms would be stopped at the bottom of GrLs. The carbon atoms at the top of GrLs were difficult to be displaced as shown in Fig. 5(e). Eventually, defects and atom displacement did not occur in the upper bulk region of Cu/8Gr/Cu, which was consistent with the data shown in Figs. 3(e) and 4(e). Therefore, the penetrable atoms and displaced carbon atoms of the top graphene plane are the sources that cause damage to their upper bulk region. The ultra-strength C–C bonds in the graphene

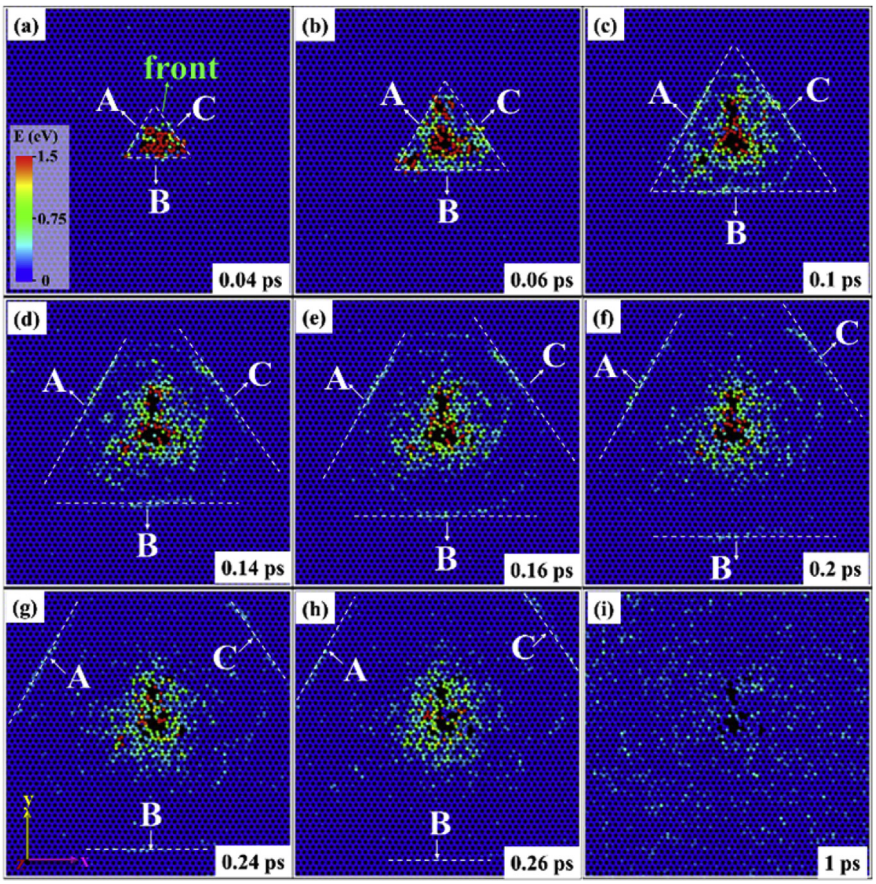

Fig. 8. Distributions of the kinetic energy of the third graphene plane in the Cu/5Gr/Cu at (**a**) 0.04, (**b**) 0.06, (**c**) 0.1, (**d**) 0.14, (**e**) 0.16, (**f**) 0.2, (**g**) 0.24, (**h**) 0.26, and (**i**) 1 ps, respectively. These images are visualised by carbon atoms coloured according to their kinetic energy. The three different directions of propagation are labelled A, B, and C, respectively. The front of each direction is marked by a white dashed line.

plane and the more numerous layers of graphene can curb the sources.

4.2. Lower bulk region of CGNC

Initially, displacement cascades induced by PKA diffuse kinetic copper atoms of the lower bulk region in all directions. Apart from those penetrable atoms, the copper atoms with the same direction of motion as that of PKA exhibit higher energy than that of other atoms according to the mechanics of one-dimensional elastic collisions [37]. This effect causes significant damage to the lower bulk region in the thermal spike phase. Once these atoms migrate to their nearest graphene plane, they are very likely to recoil into the lower bulk region because of the strong intercept force exerted by the graphene. This phenomenon will induce damage to the lower bulk region once again. Fig. 6 shows the evolution of atom displacement in the lower bulk region and its nearest graphene plane in the Cu/Gr/Cu and Cu/5Gr/Cu, respectively. The two models are selected for ease of understanding of the effects of the layers of graphene on defects and atom displacement in the lower bulk region. Only the bottom graphene is shown because of its direct influence on the recoil of copper atoms. In Fig. 6, the process that kinetic copper atoms undergo a reversed direction of motion is shown. The number of recoiled copper atoms reaches its maximum value in the time interval from 0.12 to 0.16 ps as shown in the yellow ovals of Fig. 6(d) and (i). Displacement cascades in the lower bulk region are then activated as shown in the dotted green box.

However, the scale of recoiled atoms in their lower bulk region is a significant difference between Cu/Gr/Cu and Cu/5Gr/Cu as shown in Fig. 6. More recoiled atoms occur in the gap between graphene and copper in the Cu/Gr/Cu. This phenomenon may be the main reason for more defects and atom displacement in the lower bulk region of Cu/Gr/Cu. The speculation is explained as follows. The GrL is subjected to the severe knock-on effect of kinetic copper atoms because of the few layers of graphene in Cu/Gr/Cu. Significant damage subsequently occurs in the GrL of Cu/Gr/Cu as verified by these disordered carbon atoms shown in Fig. 6(a–e); however, more damage to the GrL will weaken the intercept force exerted by the GrL on the kinetic copper atoms. These copper atoms still exhibit a high kinetic energy. Moreover, more disordered carbon atoms in the damaged region of the GrL will increase the probability of recoil of a kinetic copper atom. As a result, more recoiled atoms occur in the Cu/Gr/Cu and most of them exhibit a higher energy relative to those in other CGNCs. These recoiled atoms readily damage the lower bulk region. Differing from the Cu/Gr/Cu, the more numerous layers of graphene in the Cu/5Gr/Cu cause the knock-on of kinetic copper atoms to be shared by all of the graphene planes. In other words, a large amount of kinetic energy is propagated towards the upper graphene planes. Thus, the damage to the bottom graphene plane of Cu/5Gr/Cu is less. The bottom graphene plane still exhibits the strong intercept force effect on kinetic copper atoms as shown by the green bowing curves in Fig. 6(h–j). Eventually, the recoil probability of a kinetic copper atom is reduced. Most kinetic copper atoms are then moderated and the less damage suffered by the Cu/5Gr/Cu. Therefore, the increasing number of layers of graphene in CGNC will reduce the

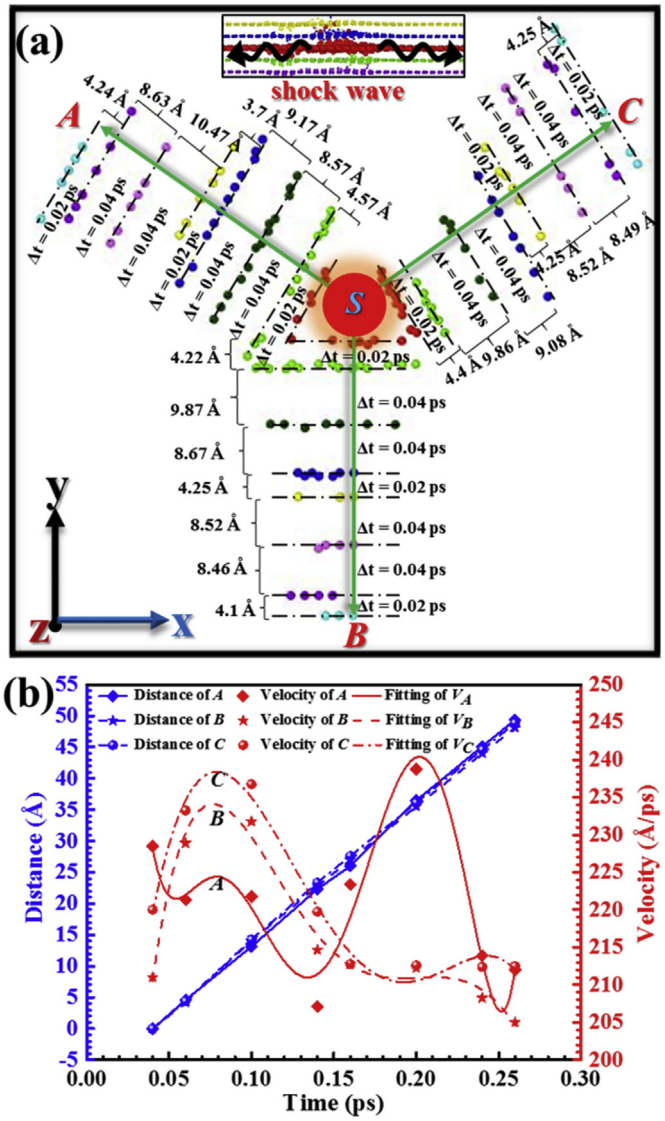

Fig. 9. (**a**) A schematic diagram showing the fronts of three different directions of propagation (A, B, and C) at different moments, which is extracted from Fig. 8. Each front position is marked by several carbon atoms, which are connected by a black dotted line. The movement distance and time interval between two adjacent fronts are also given. (**b**) Movement distance *versus* time relating to the fronts of propagation converted from panel (a). Three curves of velocity *versus* time are given by a derivative of the movement distance.

number of recoiled copper atoms and induce less damage as shown in Figs. 3(e) and 4(e).

4.3. Cu–C_gr interface region

Kinetic copper atoms from the lower bulk region, including penetrable atoms and recoiled atoms, frequently strike their GrLs. Large amounts of kinetic energy are then transferred to the GrLs in the thermal spike phase. As mentioned above, the displaced carbon atoms in the GrLs can hardly get rid of the C–C bonds of graphene, therefore, this kinetic energy is mainly stored in the GrLs. However, the significant amount of energy remaining in the GrLs will cause the system to be unstable. Thus, the ways of absorbing the kinetic energy of the GrLs without disordering a CGNC system need to be determined. Two mechanisms may be feasible: on the one hand, kinetic copper atoms will induce the displacement of carbon atoms in the GrLs. The displaced carbon atoms will continue to knock on other carbon atoms. Being fettered by the GrLs, kinetic carbon atoms cannot leave their GrLs and will be continually reflected between different graphene planes until their kinetic energy has been completely dissipated. Eventually, many dangling atoms remain in the GrLs [38]. To observe the reflected tracks of carbon atoms more clearly, Cu/5Gr/Cu is selected here. The evolution of atom displacement in the GrLs is shown in Fig. 7: kinetic carbon atoms are seen to have their kinetic energy dissipated by successive reflections.

On the other hand, a shock wave in each graphene plane may be triggered by the frequent collisions because of the two-dimensional planar structure of graphene. The shock wave will propagate along each graphene plane. The third graphene plane of Cu/5Gr/Cu is selected to explore this event. The evolution of kinetic energy in the graphene plane is shown in Fig. 8. Note that the choice of the graphene plane is arbitrary and used only to display the effect. In Fig. 8, each snapshot represents the distribution of kinetic energy of the graphene plane at different moments as visualised by the atoms coloured according to their kinetic energy. A source of shock wave occurs in the graphene plane at approximately 0.04 ps as shown by the red atoms (Fig. 8(a)). The energy of this shock wave mainly propagates in three different directions (A, B, and C). The kinetic carbon atoms at the front of each direction are marked by a white dashed line. At approximately 0.3 ps, the process of energy diffusion is almost completed. Eventually, the energy of the shock wave is divided among all of carbon atoms as shown in Fig. 8(h).

To obtain the underlying mechanism of energy dissipation, the front positions of three directions at different moments are extracted from Fig. 8. The movement distance between the two adjacent fronts for each direction is calculated as shown in Fig. 9(a). Then, these abstract numerals in Fig. 9(a) are converted to three curves of movement *versus* time (Fig. 9(b)). The front of each direction at 0.04 ps is regarded as the starting point of the motion. Each curve is then differentiated and eventually, three curves of velocity *versus* time are obtained. The velocity at the front of each direction reaches approximately 20 km/s. This value is four times as fast as that of UO_2 as found by Li et al. [39]. The velocity presents an S-shaped curve similar to that of a damped vibration [37] that also attenuates. The results highlight the role of graphene in quickly dissipating kinetic energy induced by irradiation.

5. Conclusions

The effects of GrLs on the radiation resistance of CGNC were investigated by classical molecular dynamics simulations. The main role of the GrLs is to weaken the formation, growth, and intensity of displacement cascades of CGNC. These effects are mainly reflected in the formation time of the defect count peak, the scale of the displacement cascade, and the complexity of the thermal spike region compared with those of pure copper. The behaviour directly causes the defect counts in the thermal spike phase of CGNC to decrease, accelerating the cooling, and eventually leaving very few surviving defects in the material. These phenomena become obvious with increasing numbers of layers of graphene in CGNC. For example, the defects and atom displacement in both the lower, and upper, bulk regions decreased with the increasing number of layers of graphene. The reasons for this behaviour were as follows:

1) The ultra-strength C–C bonds in the graphene plane caused a decrease in the probability that copper atoms with high energy from the lower bulk region continued inducing cascade collisions in their upper bulk region. Moreover, the displaced carbon atoms in the GrLs of each CGNC cannot escape from their GrLs.

This phenomenon caused only slight damage to the upper bulk region;

2) With the increasing number of layers of graphene, recoiled copper atoms in the lower bulk region would decrease in number, which would reduce the amount of damage suffered by the lower bulk region;
3) The propagation of kinetic energy along the graphene planes, together with the successive reflections of carbon atoms between graphene planes, would accelerate the dissipation of kinetic energy and thus reduced the damage to the entire system.

Studies have demonstrated that the expansion of the thermal spike region will aggravate the atom mixture between different types of elements under irradiation [40,41], and even trigger a phase transition in some materials [2,4,42,43]. Therefore, the fact that GrLs can significantly reduce such adverse effects, suggested the potentialities of the composites to be exploited. This finding may provide a pathway to the prevention of material degradation in extreme radiation environments by use of controlling GrLs.

Acknowledgement

This work was supported by the Funding of Jiangsu Innovation Programme for Graduate Education (Grant No. KYLX16_0350), the Fundamental Research Funds for the Central Universities (Grant No. NJ20150021), and the Priority Academic Programme Development of Jiangsu Higher Education Institutions.

Appendix A. Supplementary data

Supplementary data related to this chapter can be found at http://dx.doi.org/10.1016/j.jnucmat.2017.06.023.

References

[1] S.J. Zinkle, J.T. Busby, Structural materials for fission & fusion energy, Mater. Today 12 (2009) 12–19.
[2] I.J. Beyerlein, A. Caro, M.J. Demkowicz, N.A. Mara, A. Misra, B.P. Uberuaga, Radiation damage tolerant nanomaterials, Mater. Today 16 (2013) 443–449.
[3] B.D. Wirth, G.R. Odette, J. Marian, L. Ventelon, J.A. Young-Vandersall, L.A. Zepeda-Ruiz, Multiscale modeling of radiation damage in Fe-based alloys in the fusion environment, J. Nucl. Mater 329 (2004) 103–111.
[4] E.G. Fu, M. Caro, L.A. Zepeda-Ruiz, Y.Q. Wang, K. Baldwin, E. Bringa, M. Nastasi, A. Caro, Surface effects on the radiation response of nanoporous Au foams, Appl. Phys. Lett. 101 (2012) 191607.
[5] X. Bai, A.F. Voter, R.G. Hoagland, M. Nastasi, B.P. Uberuaga, Efficient annealing of radiation damage near grain boundaries via interstitial emission, Science 327 (2010) 1631–1634.
[6] I.J. Beyerlein, M.J. Demkowicz, A. Misra, B.P. Uberuaga, Defect-interface interactions, Prog. Mater. Sci. 74 (2015) 125–210.
[7] W.Z. Han, M.J. Demkowicz, E.G. Fu, Y.Q. Wang, A. Misra, Effect of grain boundary character on sink efficiency, Acta Mater 60 (2012) 6341–6351.
[8] F. Chen, X. Tang, Y. Yang, H. Huang, D. Chen, Investigation of structural stability and magnetic properties of Fe/Ni multilayers irradiated by 300 keV Fe^{10+}, J. Nucl. Mater 452 (2014) 31–36.
[9] Y. Chen, N. Li, D.C. Bufford, J. Li, K. Hattar, H. Wang, X. Zhang, In situ study of heavy ion irradiation response of immiscible Cu/Fe multilayers, J. Nucl. Mater 475 (2016) 274–279.
[10] B.P. Uberuaga, L.J. Vernon, E. Martinez, A.F. Voter, The relationship between grain boundary structure, defect mobility, and grain boundary sink efficiency, Sci. Rep. 5 (2015) 9095.
[11] D. Chen, J. Wang, T. Chen, L. Shao, Defect annihilation at grain boundaries in alpha-Fe, Sci. Rep. 3 (2013) 1450.
[12] J. Hwang, T. Yoon, S.H. Jin, J. Lee, T. Kim, S.H. Hong, S. Jeon, Enhanced mechanical properties of graphene/copper nanocomposites using a molecular-level mixing process, Adv. Mater 25 (2013) 6724–6729.
[13] S. Feng, Q. Guo, Z. Li, G. Fan, Z. Li, D. Xiong, Y. Su, Z. Tan, J. Zhang, D. Zhang, Strengthening and toughening mechanisms in graphene-Al nanolaminated composite micro-pillars, Acta Mater 125 (2017) 98–108.
[14] Y. Kim, J. Lee, M.S. Yeom, J.W. Shin, H. Kim, Y. Cui, J.W. Kysar, J. Hone, Y. Jung, S. Jeon, S.M. Han, Strengthening effect of single-atomic-layer graphene in metal–graphene nanolayered composites, Nat. Commun. 4 (2013) 2114.
[15] T. Wejrzanowski, M. Grybczuk, M. Chmielewski, K. Pietrzak, K.J. Kurzydlowski, A. Strojny-Nedza, Thermal conductivity of metal-graphene composites, Mater. Des. 99 (2016) 163–173.
[16] D. Prasai, J.C. Tuberquia, R.R. Harl, G.K. Jennings, K.I. Bolotin, Graphene: corrosion-inhibiting coating, ACS Nano 6 (2012) 1102–1108.
[17] Y. Kim, J. Baek, S. Kim, S. Kim, S. Ryu, S. Jeon, S.M. Han, Radiation resistant vanadium-graphene nanolayered composite, Sci. Rep. 6 (2016) 24785.
[18] S. Si, W. Li, X. Zhao, M. Han, Y. Yue, W. Wu, S. Guo, X. Zhang, Z. Dai, X. Wang, X. Xiao, C. Jiang, Significant radiation tolerance and moderate reduction in thermal transport of a tungsten nanofilm by inserting monolayer graphene, Adv. Mater 29 (2016) 1604623.
[19] T.L. Yang, L. Yang, H. Liu, H.L. Zhou, S.M. Peng, X.S. Zhou, F. Gao, X.T. Zu, Ab initio study of stability and migration of point defects in copper-graphene layered composite, J. Alloy. Compd. 692 (2017) 49–58.
[20] H. Huang, X. Tang, F. Chen, Y. Yang, J. Liu, H. Li, D. Chen, Radiation damage resistance and interface stability of copper–graphene nanolayered composite, J. Nucl. Mater 460 (2015) 16–22.
[21] H. Huang, X. Tang, F. Chen, J. Liu, H. Li, D. Chen, Graphene damage effects on radiation-resistance and configuration of copper–graphene nanocomposite under irradiation: a molecular dynamics study, Sci. Rep. 6 (2016) 39391.
[22] S.J. Stuart, A.B. Tutein, J.A. Harrison, A reactive potential for hydrocarbons with intermolecular interactions, J. Chem. Phys. 112 (2000) 6472–6486.
[23] W. Li, L. Liang, S. Zhao, S. Zhang, J. Xue, Fabrication of nanopores in a graphene sheet with heavy ions: a molecular dynamics study, J. Appl. Phys. 114 (2013) 234304.
[24] Y. Rosandi, M.L. Nietiadi, H.M. Urbassek, Subsurface channeling of keV ions between graphene layers: molecular dynamics simulation, Phys. Rev. B 91 (2015) 125441.
[25] J.B. Wallace, D. Chen, L. Shao, Carbon displacement-induced single carbon atomic chain formation and its effects on sliding of SiC fibers in SiC/graphene/SiC composite, Mater. Res. Lett. 4 (2016) 55–61.
[26] M.J. Demkowicz, R.G. Hoagland, Simulations of collision cascades in Cu–Nb layered composites using an eam interatomic potential, Int. J. Appl. Mech. 1 (2009) 421–442.
[27] S.P. Huang, D.S. Mainardi, P.B. Balbuena, Structure and dynamics of graphite-supported bimetallic nanoclusters, Surf. Sci. 545 (2003) 163–179.
[28] S. Plimpton, Fast parallel algorithms for short-range molecular dynamics, J. Comput. Phys. 117 (1995) 1–19.
[29] A. Stukowski, Visualization and analysis of atomistic simulation data with OVITO–the Open Visualization Tool, Model Simul. Mater. S. C. 18 (2009) 015012.
[30] K. Nordlund, M. Ghaly, R.S. Averback, M. Caturla, T. Diaz de la Rubia, J. Tarus, Defect production in collision cascades in elemental semiconductors and fcc metals, Phys. Rev. B 57 (1998) 7556.
[31] L.K. Béland, Y.N. Osetsky, R.E. Stoller, The effect of alloying nickel with iron on the supersonic ballistic stage of high energy displacement cascades, Acta. Mater 116 (2016) 136–142.
[32] H.J. Christie, M. Robinson, D.L. Roach, D.K. Ross, I. Suarez-Martinez, N.A. Marks, Simulating radiation damage cascades in graphite, Carbon 81 (2015) 105–114.
[33] J.A. Hinks, S.J. Haigh, G. Greaves, F. Sweeney, C.T. Pan, R.J. Young, S.E. Donnelly, Dynamic microstructural evolution of graphite under displacing irradiation, Carbon 68 (2014) 273–284.
[34] A.M. James, M.P. Lord, Macmillan's Chemical and Physical Data, Macmillan, London, 1992.
[35] W.G. Wolfer, Fundamental Properties of Defects in Metals, in: R.J.M. Konings (Ed.), Comprehensive Nuclear Materials, Elsevier, Amsterdam, 2012, pp. 1–45.
[36] E.P. Bellido, J.M. Seminario, Molecular dynamics simulations of ion-bombarded graphene, J. Phys. Chem. C 116 (2012) 4044–4049.
[37] A.F. Rex, R. Wolfson, Essential College Physics, first ed., Addison-Wesley, Boston, 2009.
[38] A. Chartier, L.V. Brutzel, B. Pannier, P. Baranek, Atomic scale mechanisms for the amorphisation of irradiated graphite, Carbon 91 (2015) 395–407.
[39] Z. Li, D. Chen, L. Shao, Melting and shock wave creation in uranium oxide due to Coulomb explosion after a pulsed ionization, Nucl. Instrum. Meth. B 358 (2015) 65–71.
[40] L. Zhang, M.J. Demkowicz, Radiation-induced mixing between metals of low solid solubility, Acta Mater 76 (2014) 135–150.
[41] T. Lee, A. Caro, M.J. Demkowicz, Atomistic modeling of radiation-induced disordering and dissolution at a Ni/Ni3Al interface, J. Mater. Res. 30 (2015) 1456–1463.
[42] W.J. Weber, R.C. Ewing, L.M. Wang, The radiation-induced crystalline-to-amorphous transition in zircon, J. Mater. Res. 9 (1994) 688–698.
[43] G. Thomas, H. Mori, H. Fujita, R. Sinclair, Electron irradiation induced crystalline amorphous transitions in Ni-Ti alloys, Scr. Metall. 16 (1982) 589–592.